

A test of cosmic distance duality relation using SPT-SZ galaxy clusters, Type Ia supernovae, and cosmic chronometers

Kamal Bora* and Shantanu Desai†

Department of Physics, Indian Institute of Technology, Hyderabad, Kandi, Telangana-502285, India

(Dated: April 5, 2021)

We carry out a test of the cosmic distance duality relation using a sample of 58 SPT-SZ clusters, along with X-ray measurements from XMM-Newton. To carry out this test, we need an estimate of the luminosity distance (D_L) at the redshift of the cluster. We use three independent methods for this purpose: directly using D_L from the closest Type Ia Supernovae from the Union 2.1 sample, non-parametric reconstruction of D_L using the same Union 2.1 sample, and finally using $H(z)$ measurements from cosmic chronometers and reconstructing D_L using Gaussian Process regression. We use four different functions to characterize the deviations from CDDR. All our results for these (4×3) analyses are consistent with CDDR to within $1 - 3\sigma$.

I. INTRODUCTION

One of the most fundamental tenet in Cosmology is the cosmic distance duality relation (CDDR, hereafter) between the angular diameter distance (D_A) and the luminosity distance (D_L), which is sometimes also known as the Etherington relation [1, 2]. This relation is given by:

$$\eta(z) \equiv \frac{D_L}{D_A(1+z)^2} = 1 \quad (1)$$

The CDDR involves three assumptions [3, 4]: spacetime is endowed with a metric theory of gravity; photons propagate along null geodesics; and the total number of photons is conserved. The CDDR relation is one of the edifice of the standard Λ CDM model [5]. Although, the Λ CDM is very successful in describing the large scale structure from CMB and other probes [6], a number of tensions have crept up in recent years, such as the Hubble constant tension between low redshift and high redshift probes [7–9], σ_8 tension [10], Lithium-7 problem in Big-Bang Nucleosynthesis [11], core-cusp and missing satellites problem [12, 13], failure to detect cold dark matter in the laboratory [14], failure to explain regularities in cosmic structure at galactic scales such as the radial acceleration relation and Baryonic Tully-Fisher relation [15, 16]. Therefore, a large number of works have tried to test the CDDR in a model-independent way using a variety of astrophysical probes [4, 17–30].

In this work, we shall use galaxy cluster observations observed in the microwave, via Sunyaev-Zeldovich effect (SZ, hereafter) and X-rays to test CDDR. Galaxy clusters are the most massive virialized collapsed objects in the universe and are wonderful laboratories for a whole range of topics in Cosmology, galaxy evolution, and fundamental Physics [31–34]. The first test of CDDR using galaxy clusters was done by [17]. They used the

X-ray and SZ observations from [35] to test the validity of the CDDR, and obtained η close to unity at 2σ level. Later, de Bernardis et al. [18] did a similar test using the angular diameter distance of 38 galaxy clusters from Chandra X-ray data and SZ observations from the OVRO and BIMA interferometric arrays. They reported $\eta(z) = 0.97 \pm 0.03$, which implies that there is no violation of CDDR at 1σ . Holanda et al. [36] then implemented the first model-independent cosmological test of CDDR by using joint SZ and X-ray surface brightness measurements, along with Type Ia SNe from the Constitution data [37]. Here, they used two different sample of galaxy clusters from [38] and [39], corresponding to elliptical and spherical geometry, respectively. For their analyses, they used two different parametric forms for $\eta(z)$. For elliptical geometry, they obtained $\eta_0 = -0.28 \pm 0.44$ (2σ) and -0.43 ± 0.60 (2σ) for the two different parametrizations used. However for spherical geometry, they obtained $\eta_0 = -0.42 \pm 0.34$ (3σ) and $\eta_0 = -0.66 \pm 0.50$ (3σ) for linear and non-linear parametric forms respectively. Hence, they concluded that the elliptical geometry of galaxy clusters is compatible with the validity of the distance duality relation but not the spherical geometry. Gonçalves et al. [40] used X-ray f_{gas} data along with SNe Ia from Union 2 compilation [41]. Here, they again used the two samples of galaxy clusters [38, 39]. They found that one of the samples [38] is consistent with CDDR, whereas the other sample [39] shows a 3.5σ deviation from CDDR. Later, Holanda et al. [42] reported no violation of CDDR using a combination of SZ and X-ray gas mass fraction data [38]. Liang et al. [43] tested the distance duality relation using a sample of 38 angular diameter distances from galaxy clusters assuming the spherical model [44], along with SNe Ia data from Union 2 compilation [41]. They found no evidence for the violation of CDDR at $1 - 2\sigma$, depending on the parameterization used. Yang et al. [45] did a model independent test of CDDR using the angular diameter distances from two different cluster samples [44, 46] corresponding to spherical and elliptical geometry, respectively, in conjunction with the Union 2 SNe Ia sample [41]. However, instead of using the SNe Ia D_L from the distance mod-

*E-mail: ph18resch11003@iith.ac.in

†E-mail: shntn05@gmail.com

ulus, they used the original SNe data for the rest-frame peak magnitudes and other parameters describing the influence of intrinsic color and reddening by dust. They obtained no violation of CDDR at 1σ for both the elliptical and spherical cluster samples, but they concluded that the spherical model [44] can better describe the intrinsic geometry of the clusters as compared to the elliptical one [46], if the CDDR relation is valid. Santos-da-Costa et al. [47] used two different methods to test CDDR using 38 angular diameter distances obtained from [44] (which was also used in earlier tests of CDDR [45]), along with their f_{gas} measurements [38] spanning the redshift range $0.14 < z < 0.89$. This was then compared with an independent estimate of the angular diameter distance, reconstructed using $H(z)$ data from cosmic chronometers and BAO. The departure from CDDR was reconstructed in a non-parametric manner. Both the methods were consistent with the validity of CDDR at 1σ . Holanda and Pereira [48] studied the temporal variation of fine structure constant, modified distance duality relation, and the modified evolution law of the cosmic microwave background radiation by using the angular diameter distances to 29 galaxy clusters [44], Union2.1 Type Ia SNe compilation [49], and 38 T_{CMB} measurements [50, 51]. All of these variants/modifications of the Standard Model arise naturally from a class of modified gravity theories, which break the Einstein Equivalence Principle. Their results are consistent with no violation of these laws at 1σ . (See also [52, 53] for similar follow-up studies). Holanda et al. [54] (H19, hereafter) have also done a study of the validity of CDDR relation using the $Y_{SZ} - Y_X$ scaling relation for 61 Planck ESZ clusters jointly with deep XMM-Newton archive observations in the redshift range $0.044 \leq z \leq 0.444$ [55], along with Type Ia SNe from the Pantheon compilation [56]. They reported no violation of CDDR at 1.5σ . Most recently, da Silva et al. [57] did a Bayesian model comparison assuming CDDR violation for different forms of $\eta(z)$ using two sets of data namely SNe Ia [56] + angular diameter distances from galaxy clusters [46] and SNe Ia [56] + gas mass fraction data [58]. Their results showed agreement with CDDR at 2σ for SNe Ia and angular diameter distances from galaxy clusters sample, and at 1σ for SNe Ia along with the gas mass fraction measurements.

In this work, we shall use SZ selected clusters from the South Pole telescope in conjunction with X-ray followup observations from the XMM-Newton telescope to test for a violation of CDDR. This paper is structured as follows. In Sec. II, we briefly explain the basic theory behind the X-ray and SZ observables used to test CDDR. In Sec. III, we describe our cluster sample. Sec. IV discusses the calculation of D_L using three independent methods. Details of our analysis and results can be found in Sec. V. We conclude in Sec. VI.

II. METHODOLOGY

The Inverse Compton scattering between the CMB photons and the hot electrons present in the intra-cluster medium causes a spectral distortion of the CMB black body spectrum [59–62]. This spectral distortion is known as the SZ effect. It is nearly independent of redshift, and hence can detect galaxy clusters upto very high redshifts. The distortion is measured by a parameter, called Compton- y parameter which is given by [60, 61],

$$y = \frac{\sigma_T k_B}{m_e c^2} \int n_e T dl, \quad (2)$$

where, T is the electron temperature, m_e is mass of the electron, c is the speed of light, n_e is the number density of electrons, k_B is the Boltzmann constant, and σ_T is the Thompson scattering cross section which is given by,

$$\sigma_T = \frac{8\pi}{3} \left(\frac{e^2}{m_e c^2} \right)^2 = \frac{8\pi}{3} \left(\frac{\hbar^2 \alpha^2}{m_e^2 c^2} \right) \quad (3)$$

If we model the variation in α as $\alpha(z) \equiv \alpha_0 \phi(z)$, where α_0 is the present value of α , the fractional variation in α can be written as,

$$\frac{\Delta\alpha}{\alpha_0} = \phi(z) - 1 \quad (4)$$

We assume that the intra-cluster medium is an ideal gas, with its equation of state given by $P = n_e k_B T$, where P refers the pressure of the intra-cluster gas. The relation between the integrated Compton parameter over the solid angle (Y_{SZ}) and the angular diameter distance to the cluster (D_A) is given by [63]:

$$Y_{SZ} D_A^2 \propto \phi(z)^2 \quad (5)$$

The hot intra-cluster gas emits X-rays mainly through thermal bremsstrahlung process [31, 64]. If $M_g(R)$ is the gas mass within radius R and T_X is the X-ray temperature then the average thermal energy of the cluster gas is given by [65],

$$Y_X = M_g(R) T_X \quad (6)$$

Also the gas mass $M_g(R)$ depends on α as [40, 66, 67],

$$M_g(< \theta) \propto \phi(z)^{-3/2} D_L D_A^{3/2}, \quad (7)$$

where D_L is the luminosity distance. D_L and D_A are connected via CDDR, $D_L = (1+z)^2 D_A$ [1]. [68, 69] showed that any variation in α is interlinked with a violation of CDDR. If we parameterize a violation of CDDR using $D_L \equiv \eta(z)(1+z)^2 D_A$, then Y_X scales with α and $\eta(z)$ as [63, 67],

$$Y_X \propto \phi(z)^{-3/2} \eta(z) \quad (8)$$

For a wide class of modified theories of gravity [68, 70], the Einstein's equivalence principle breaks down due to the coupling of the scalar field with the electromagnetic sector. In these theories, $\alpha(z)$ and $\eta(z)$ are related according to $\alpha(z) = (\eta(z))^2$. Y_{SZ} and Y_X can then be rewritten in terms of $\eta(z)$ as:

$$Y_{SZ}D_A^2 \propto \eta(z)^4 \quad (9)$$

and

$$Y_X \propto \eta(z)^{-2} \quad (10)$$

Y_{SZ} and Y_X are two different proxies for the thermal energy of the cluster [71], so the ratio $Y_{SZ}D_A^2/C_{XSZ}Y_X$ is expected to be constant with redshift, since both these quantities scale with redshift and mass in exactly the same way. Simulations show that this ratio is constant with 5–15% scatter [72–76]. The ratio would be exactly one or constant with redshift for clusters with isothermal or universal temperature profiles [66, 67, 77]. From Eq. 9 and 10, this ratio scales with $\eta(z)$ as:

$$\frac{Y_{SZ}D_A^2}{Y_X C_{XSZ}} = C\eta(z)^6 \quad (11)$$

where $C_{XSZ} \approx 1.416 \times 10^{-19} \left(\frac{Mpc^2}{M_\odot keV} \right)$ and C is an arbitrary constant, which contains all the cluster astrophysics and is equal to one for an isothermal profile [67].

From Eq. 6 and 7, one can see that Y_X scales with D_A according $Y_X \propto D_A^{5/2}$, if we assume a flat Λ CDM cosmology and the validity of CDDR. Following H19, we multiply Y_X by $D_A^{5/2}/(D_A^{ref})^{5/2}$ in order to eliminate the dependency of $M_g(R)$ with respect to the fiducial cosmology. Hence we get,

$$\frac{Y_{SZ}D_A^2(D_A^{ref})^{5/2}}{Y_X C_{XSZ}D_A^{5/2}} = C\eta(z)^6 \quad (12)$$

Since we want to carry out a test of CDDR in a model-agnostic fashion, we recast this equation in terms of D_L

by parameterizing any violation of CDDR using $\eta(z)$ defined in Eq. 1.

So Eq. 12 can be written as,

$$\frac{Y_{SZ}(D_A^{ref})^{5/2}(1+z)}{Y_X C_{XSZ}D_L^{1/2}} = C\eta(z)^{11/2} \quad (13)$$

III. CLUSTER SAMPLE

For our analysis, we use Y_{SZ} and Y_X for 58 SPT-SZ selected galaxy from Bulbul et al. [78]. The SZ data have been taken from the South Pole Telescope (hereafter SPT) which is a 10 m millimeter wave telescope located at the South Pole [79]. One of the main goals of the SPT is to find galaxy clusters using their SZ signatures upto very high redshifts. SPT has imaged the sky at three different frequencies viz. 95 GHz, 150 GHz, and 220 GHz [79], and carried out a 2500 square degree survey between 2007 to 2011. A total of 516 galaxy clusters have been detected in this survey, with a mass threshold of $3 \times 10^{14} M_\odot$ and spanning the redshifts upto 1.8 [80, 81]. Many dedicated optical surveys, e.g. DES [82], BCS [83] as well as targeted observations [84] have followed-up the SPT cluster candidates in order to determine their photometric redshifts. Here, we have also used the X-ray observations (by XMM-Newton) for 58 of these clusters, in the redshift range $0.2 \leq z \leq 1.5$ [78]. The Y_X parameter from XMM-Newton measurement has been measured at R_{500} . The Y_{SZ} measurements provided by SPT have been obtained by averaging over a cylindrical volume within an aperture radius of $0.75R'$ [80]. Since, the Y_{SZ} parameter defined in Eq. 9 needs to be averaged over a spherical volume, we need to convert the cylindrically averaged Y_{SZ} to a spherically averaged Y_{SZ} at R_{500} , for which we have used the following conversion method [85, 86]:

$$Y_{cyl}(R_1) = Y_{sph}(R_b) - \frac{\sigma_T}{m_e c^2} \int_{R_1}^{R_b} 4\pi P(r) \sqrt{r^2 - R_1^2} r dr \quad (14)$$

$$Y_{sph}(R_2) = \frac{\sigma_T}{m_e c^2} \int_0^{R_2} 4\pi P(r) r^2 dr \quad (15)$$

where the subscripts *cyl* and *sph* indicate the Y_{SZ} parameter in cylindrical and spherical volumes, respectively. R_1 indicates the cylindrical aperture in which Y_{cyl} is measured and R_b denotes the radial extent of the cluster. We assume $R_b = 10R_{500}$, $R_1 = 0.75'R_{500}$, and

$R_2 = R_{500}$ [85]. In Eq. 15, $P(r)$ refers to the pressure

profile. To do the conversion, we have used the Univer-

sal Pressure Profile (UPP) [85]¹ for $P(r)$. Hence, from Eq. 14 and Eq. 15, we can estimate the ratio of $Y_{sph}(R_{500})$ to $Y_{cyl}(0.75'D_A)$. By using this ratio one can estimate $Y_{sph}(R_{500})$ for every SPT-SZ cluster.

IV. CALCULATION OF LUMINOSITY DISTANCE D_L

We use three different methods to estimate the D_L for each cluster. We now describe each of these methods.

A. Method 1: Using a redshift cut

We use Type Ia SNe samples from the Union 2.1 compilation [49], which consists of 580 Type Ia supernovae data spanning the redshift range $0.015 \leq z \leq 1.414$ (with median redshift of $z \approx 0.294$) in order to estimate D_L for the SPT-SZ sample by choosing the closest SNe corresponding to every cluster. Similar to H19, we use the following cut on the supernova redshift (z_{SNe}) for choosing the closest type Ia SNe corresponding to a cluster with redshift z : $|z - z_{SNe}| \leq 0.005$. For most galaxy clusters, there are multiple supernovae satisfying the above cut. To determine the D_L and its error at the cluster location in such cases, we calculate the weighted average of the distance modulus of type Ia SNe and its associated error. The luminosity distance D_L can be obtained from the distance modulus μ using the following equation:

$$D_L(z) = 10^{(\bar{\mu}(z) - 25)/5} \quad (16)$$

For six clusters, we could not find any supernovae counterparts with the aforementioned redshift cut, and these clusters were therefore culled from our sample. Thereafter, with this method, we are left with a sample of 52 clusters for our analysis.

B. Method 2: Non-parametric reconstruction using Type Ia SNe

We now adopt another method to find D_L for every cluster, by using the Gaussian Processes Regression (GPR). A Gaussian process is the generalisation of a

Gaussian distribution. It is characterized by a mean function and a covariance function (usually called the kernel function) [88]. More details about GPR can be found in our past works [89, 90]. For this work, we select the squared exponential (RBF) covariance function, which is given by:

$$K(x, \tilde{x}) = \sigma_f^2 \exp \left[\frac{-(x - \tilde{x})^2}{2l^2} \right], \quad (17)$$

It depends on two hyperparameters: σ_f and l . The length parameter l controls the smoothness of the kernel function. To reconstruct D_L at the cluster redshift, we used the `scikit-learn` module in python [91]. Fig 1 shows the reconstructed luminosity distance as a function of z using GPR. Using this non-parametric reconstruction, one can estimate D_L for every SPT-SZ cluster.

C. Method 3: Reconstruction using cosmic chronometers

Here, we used 31 $H(z)$ measurements from Li et al. [92] (same as that used in [89, 90]) spanning the redshift range $0.07 \leq z \leq 1.965$. These $H(z)$ measurements are obtained from cosmic chronometers, which provide a model agnostic estimate of the expansion history at any redshift z [93]. Using these $H(z)$ measurements, we have again used the `scikit-learn` module for GPR, to estimate $H(z)$ for any redshift. Furthermore, the reconstructed $H(z)$ data can be used to derive the luminosity distance D_L which can be written as,

$$D_L(z) = c(1+z) \int_0^z \frac{dz'}{H(z')} \quad (18)$$

where $H(z')$ is the reconstructed Hubble data. Fig 2 shows the reconstructed $H(z)$ data from chronometers as a function of z along with their 1σ and 2σ uncertainties.

A comparison plot of the luminosity distance D_L as a function of z using all the three methods is shown in Fig 3.

V. ANALYSIS AND RESULTS

In order to constrain $\eta(z)$ (as used in Eq. 13), we use the following parametric forms [68]. These were also used in H19 and other works testing for a violation of CDDR.

$$\eta(z) = 1 + \eta_0 z \quad (19)$$

$$\eta(z) = 1 + \eta_0 [z/(1+z)] \quad (20)$$

$$\eta(z) = 1 + \eta_0 \ln(1+z) \quad (21)$$

$$\eta(z) = (1+z)^{\eta_0} \quad (22)$$

For all the above parametrizations, η_0 encapsulates a possible departure from the standard CDDR, and $\eta_0 = 0$

¹ As a cross-check we also did the conversion using the BPP profile [87], but the difference in results compared to UPP is negligible, and we therefore do not report these results in this manuscript.

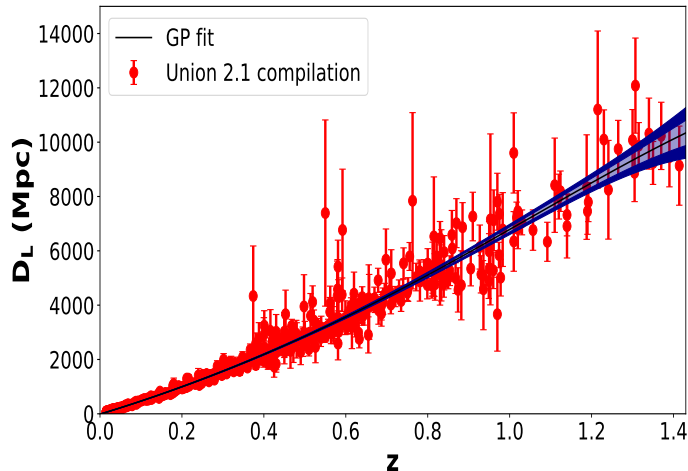


FIG. 1: Reconstruction of D_L using GPR. The red data points show the 580 Type Ia SNe taken from Union 2.1 compilation [49]. The black line indicates the best GP fit to the data along with 1σ and 2σ error bands shown by the two different shades of blue color.

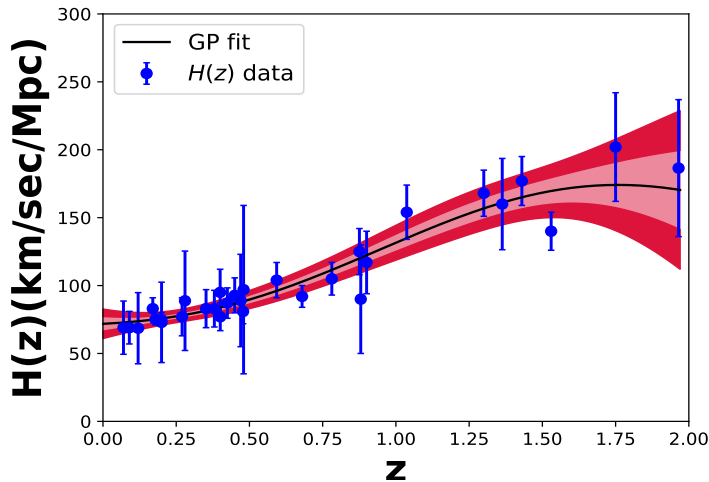


FIG. 2: Reconstruction of $H(z)$ using GPR. The blue data points represent the 31 $H(z)$ cosmic chronometer measurements compiled by Li et al. [92]. The black line indicates the best GP fit to data along with 1σ and 2σ error bands shown by the two different shades of red color.

corresponds to no CDDR violation. Table I summarizes all the possible combinations of the different methods for D_L measurements and equations for $\eta(z)$ we have studied in this work. The $Y_{SZ} - Y_X$ ratio given by Eq. 13 is shown in Fig 4 for each of the methods used for reconstructing D_L (as discussed in Sec. IV).

We now proceed to obtaining constraints on $\eta(z)$ for each of the parametrizations. The likelihood function \mathcal{L} used in our analysis is given by:

$$-2 \ln \mathcal{L} = \sum_{i=1}^N \frac{(\eta_{obs}(z_i) - C\eta(z)^{11/2})^2}{\sigma_i^2} + \sum_{i=1}^N \ln 2\pi\sigma_i^2, \quad (23)$$

where η_{obs} is obtained from Eq. 13 and σ_i denotes the total error calculated as follows:

$$\sigma_i^2 = \sigma_\eta^2 + \sigma_{int}^2 \quad (24)$$

where, σ_η^2 represents the error in η_{obs} which is calculated by propagating the errors in $Y_{SZ}, Y_X, D_L(z)$, and D_A^{ref} . We have also included an intrinsic scatter term (σ_{int}) as a free parameter, which is added in quadrature to the observational error, while maximizing the likelihood. We used the `emcee` MCMC sampler [94] to estimate the model parameters i.e. η_0 and C , by maximizing the likelihood function defined in Eq. 23.

The marginalized one-dimensional likelihoods for each

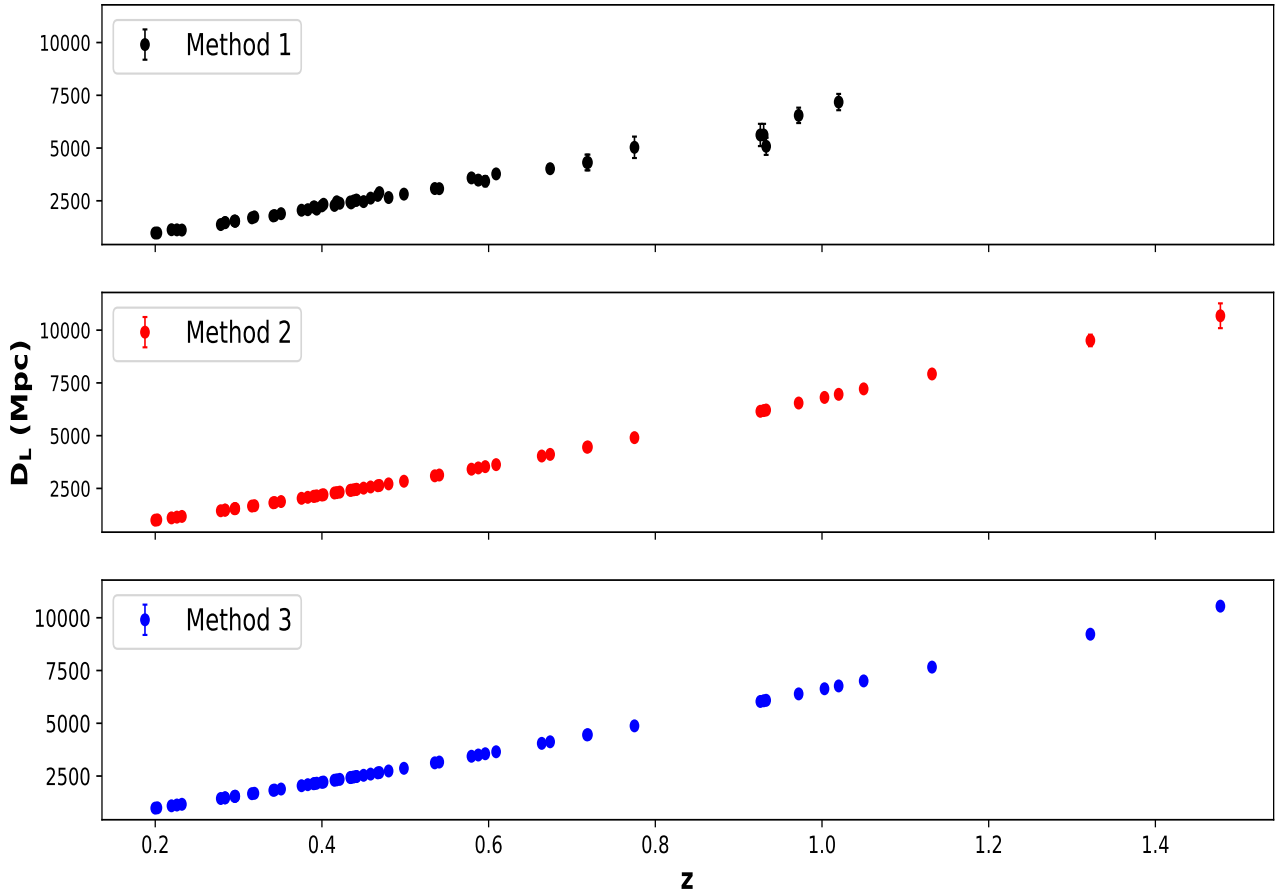


FIG. 3: A comparison of D_L for the SPT cluster sample obtained from the different methods as discussed in Sec IV. In the topmost panel (corresponding to Method 1), six clusters have been culled, since no redshift counterpart could be found based on the redshift cut used here.

of the parameters along with the 2-D 68%, 95%, and 99% credible intervals, are displayed in Fig. 5- 8 for each of the parametric forms in Eqs. 19,20,21, 22, respectively. These contour intervals are shown for Cases I-IV, corresponding to Method 1 for calculating D_L . A complete summary of all our results for the four parametric forms with each of the three methods for computing D_L is tabulated in Table II. This table also contains a summary of previous results in literature for the same parametric forms, whenever available. A graphical summary of all our results for the different cases can be found in Fig 9.

From these analyses, our main inferences are as follows. **For Case I-IV**, we find a negligible evolution of $\eta(z)$ as a function of z at 1σ . On the other hand, for the remaining cases (**V-XII**), our results show a mild discrepancy with CDDR at 1σ but are consistent with the CDDR at $2 - 3\sigma$. The largest discrepancy (2.9σ) is seen for **Case VI**, corresponding to Eq. 20, where D_L was obtained from

the non-parametric reconstruction of SNe D_L .

VI. CONCLUSIONS

In this work, we carried out a model-independent test of CDDR, along the same lines as H19. For this purpose, we used 58 SPT-SZ clusters in the redshift range $0.2 \leq z \leq 1.5$ in conjunction with X-ray measurements from XMM-Newton [78]. To get independent distance measurements at the cluster redshifts, we used Type Ia SNe [49] and $H(z)$ measurements from cosmic chronometers [92]. The observables used to test CDDR include the SZ Compto-ionization parameter (Y_{SZ}), along with its X-ray counterpart (Y_X), both of which are independent thermal energy proxies, having different scalings with $\eta(z)$ (cf. Eq. 9 and 10). The Y_{SZ} to Y_X ratio is then used to test the CDDR, which is given by Eq. 13. One input

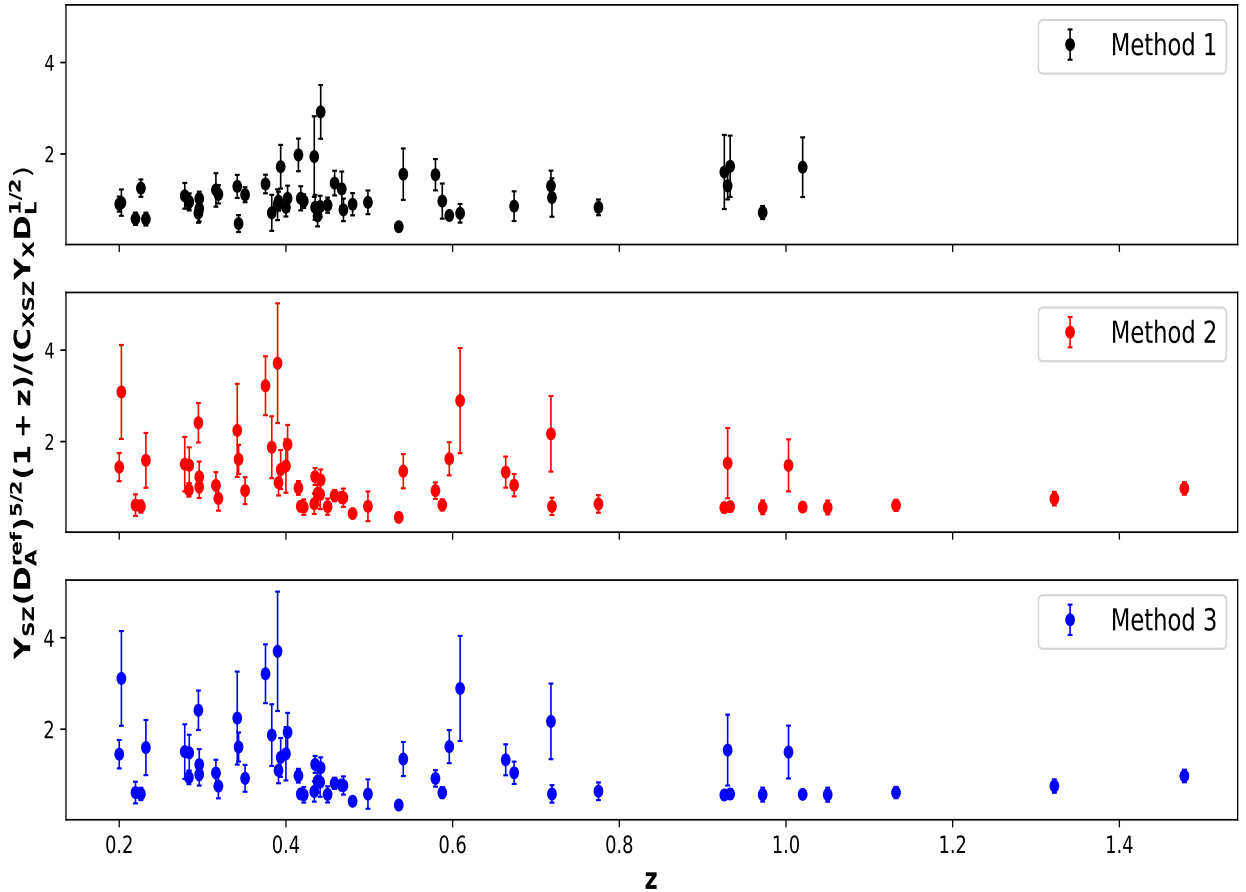


FIG. 4: A comparison of the Y_{SZ} - Y_X ratio defined in Eq. 13 for the three different methods used for calculating D_L , as described in Sec. IV.

needed for this analysis is the luminosity distance at the cluster redshift, for which we have used three independent estimators. These are summarized in Sect IV and tabulated in Table I. The dimensionless ratio of Y_{SZ} to Y_X (after suitable scalings) is shown in Fig 4 as a function of z for all the three methods used for estimating D_L .

To test the validity of CDDR, we chose different parametric forms, defined in Eqs. 19 - Eq. 22, where the parameter η_0 characterizes any departure from CDDR. Table I shows all the possible used cases studied in this work. Furthermore, to estimate the parameters in Eqs. 19 - Eq. 22, we maximize the likelihood function given by Eq 23. Our results can be found in Table II

along with a comparison with previous results. A graphical summary of all our results for CDDR (for all the cases studied) can be found in Fig 9. For Cases I-IV, the joint 2-D credible intervals for η_0 and C (a parameter in the Y_{SZ} to Y_X ratio) can be found in Fig 5 - Fig 8. Our results are consistent with no violation of CDDR at 1σ for Case I-IV and at $2\sigma - 3\sigma$ for Case V-XII. The maximum discrepancy is seen at 2.9σ for Case VI, wherein Type Ia SNe were used to calculate the luminosity distance D_L using GPR, and η_0 was calculated using the parameterization in Eq. 20.

Therefore, we conclude that there is no statistically significant evidence for a violation of CDDR, in agreement with previous results.

[1] I. M. H. Etherington, Philosophical Magazine **15**, 761 (1933).

[2] G. F. R. Ellis, General Relativity and Gravitation **39**,

Combination	Method 1	Method 2	Method 3	Eq. 19	Eq. 20	Eq. 21	Eq. 22
Case I	✓			✓			
Case II	✓				✓		
Case III	✓					✓	
Case IV	✓						✓
Case V		✓		✓			
Case VI		✓			✓		
Case VII		✓				✓	
Case VIII		✓					✓
Case IX			✓	✓			
Case X			✓		✓		
Case XI			✓			✓	
Case XII			✓				✓

TABLE I: An illustration of the different analyses used for testing CDDR.

Dataset used	Eq. 19	Eq. 20	Eq. 21	Eq. 22	Reference
Angular Dia Dist+SNe Ia	$-0.28 \pm 0.44(2\sigma)$	$-0.43 \pm 0.60(2\sigma)$	-	-	[36]
Angular Dia Dist+SNe Ia	-0.15 ± 0.17	-0.23 ± 0.24	-	-	[95]
Angular Dia Dist+SNe Ia	-0.07 ± 0.19	-0.11 ± 0.26	-	-	[20]
f_{gas}	-0.06 ± 0.16	-0.07 ± 0.24	-	-	[42]
f_{gas} +SNe Ia	$-0.03^{+1.03}_{-0.65}$	$-0.08^{+2.28}_{-1.22}$	-	-	[40]
Angular Dia Dist+SNe Ia	$-0.23 \pm 0.23(2\sigma)$	$-0.35 \pm 0.37(2\sigma)$	-	-	[43]
Angular Dia Dist+SNe Ia	$0.16^{+0.56}_{-0.39}$	-	-	-	[45]
Angular Dia Dist+ $H(z)$	$-0.10^{+0.12}_{-0.13}$	$-0.16^{+0.18}_{-0.19}$	-	-	[47]
$f_{gas}+H(z)$	$0.062^{+0.17}_{-0.15}$	$-0.17^{+0.34}_{-0.28}$	-	-	[47]
Angular Dia Dist+ f_{gas} +SNe Ia+ T_{CMB}	-0.012 ± 0.022	-0.02 ± 0.034	-0.017 ± 0.027	-0.017 ± 0.026	[53]
Angular Dia Dist+ f_{gas} +SNe Ia+ T_{CMB}	-0.011 ± 0.021	-0.015 ± 0.033	-0.013 ± 0.027	-0.013 ± 0.028	[53]
Strong Grav. Lensing+SNe Ia+GRBs	$0.00 \pm 0.10(2\sigma)$	$-0.36^{+0.37}_{-0.42}(2\sigma)$	$-0.10 \pm 0.24(2\sigma)$	$-0.16^{+0.24}_{-0.51}(2\sigma)$	[52]
Strong Grav. Lensing+SNe Ia+GRBs	$0.15 \pm 0.13(2\sigma)$	$-0.18^{+0.45}_{-0.65}(2\sigma)$	$0.22^{+0.40}_{-0.32}(2\sigma)$	$0.27^{+0.22}_{-0.38}(2\sigma)$	[52]
$Y_{SZ} - Y_X$ +SNe Ia	$0.05 \pm 0.07(2\sigma)$	$0.09 \pm 0.16(2\sigma)$	-	-	[54]
$Y_{SZ} - Y_X$ ratio+SNe Ia(Method 1)	0.008 ± 0.05	0.022 ± 0.11	0.012 ± 0.07	0.01 ± 0.07	This work
$Y_{SZ} - Y_X$ ratio+SNe Ia(Method 2)	-0.096 ± 0.04	-0.26 ± 0.09	-0.16 ± 0.06	-0.18 ± 0.07	This work
$Y_{SZ} - Y_X$ ratio+$H(z)$(Method3)	-0.094 ± 0.04	-0.26 ± 0.09	-0.16 ± 0.06	-0.18 ± 0.07	This work

TABLE II: Constraints on η_0 from previous studies using different parametric forms as defined in Eq. 19 - Eq. 22 along with our results presented in last three rows. The quoted uncertainties are at 1σ wherever not mentioned explicitly.

- 1047 (2007).
- [3] B. A. Bassett and M. Kunz, Phys. Rev. D **69**, 101305 (2004), URL <https://link.aps.org/doi/10.1103/PhysRevD.69.101305>.
- [4] J. Qin, F. Melia, and T.-J. Zhang, Mon. Not. R. Astron. Soc. **502**, 3500 (2021), 2101.05574.
- [5] B. Ratra and M. S. Vogeley, PASP **120**, 235 (2008), 0706.1565.
- [6] Planck Collaboration, N. Aghanim, Y. Akrami, M. Ashdown, J. Aumont, C. Baccigalupi, M. Ballardini, A. J. Banday, R. B. Barreiro, N. Bartolo, et al., Astron. & Astrophys. **641**, A6 (2020), 1807.06209.
- [7] E. Di Valentino, O. Mena, S. Pan, L. Visinelli, W. Yang, A. Melchiorri, D. F. Mota, A. G. Riess, and J. Silk, arXiv e-prints arXiv:2103.01183 (2021), 2103.01183.
- [8] L. Verde, T. Treu, and A. G. Riess, Nature Astronomy **3**, 891 (2019), 1907.10625.
- [9] S. Bethapudi and S. Desai, Eur. Phys. J. Plus **132**, 78 (2017), 1701.01789.
- [10] D. Benisty, Physics of the Dark Universe **31**, 100766 (2021), 2005.03751.
- [11] B. D. Fields, K. A. Olive, T.-H. Yeh, and C. Young, JCAP **2020**, 010 (2020), 1912.01132.
- [12] J. S. Bullock and M. Boylan-Kolchin, Ann. Rev. Astron. Astrophys. **55**, 343 (2017), 1707.04256.
- [13] D. H. Weinberg, J. S. Bullock, F. Governato, R. Kuzio de Naray, and A. H. G. Peter, Proceedings of the National Academy of Science **112**, 12249 (2015), 1306.0913.
- [14] D. Merritt, Studies in the History and Philosophy of Modern Physics **57**, 41 (2017), 1703.02389.
- [15] S. S. McGaugh, F. Lelli, and J. M. Schombert, Phys. Rev. Lett. **117**, 201101 (2016), 1609.05917.
- [16] S. Pradyumna, S. Gupta, S. Seeram, and S. Desai, Physics of the Dark Universe **31**, 100765 (2021), 2011.06421.
- [17] J.-P. Uzan, N. Aghanim, and Y. Mellier, Phys. Rev. D **70**, 083533 (2004), URL <https://link.aps.org/doi/10.1103/PhysRevD.70.083533>.
- [18] F. de Bernardis, E. Giusarma, and A. Melchiorri, International Journal of Modern Physics D **15**, 759 (2006), gr-qc/0606029.
- [19] S. Khedekar and S. Chakraborti, Phys. Rev. Lett. **106**, 221301 (2011), URL <https://link.aps.org/doi/10.1103/PhysRevLett.106.221301>.
- [20] Z. Li, P. Wu, and H. Yu, Astrophys. J. Lett. **729**, L14 (2011), 1101.5255.
- [21] R. Nair, S. Jhingan, and D. Jain, JCAP **2011**, 023 (2011), 1102.1065.

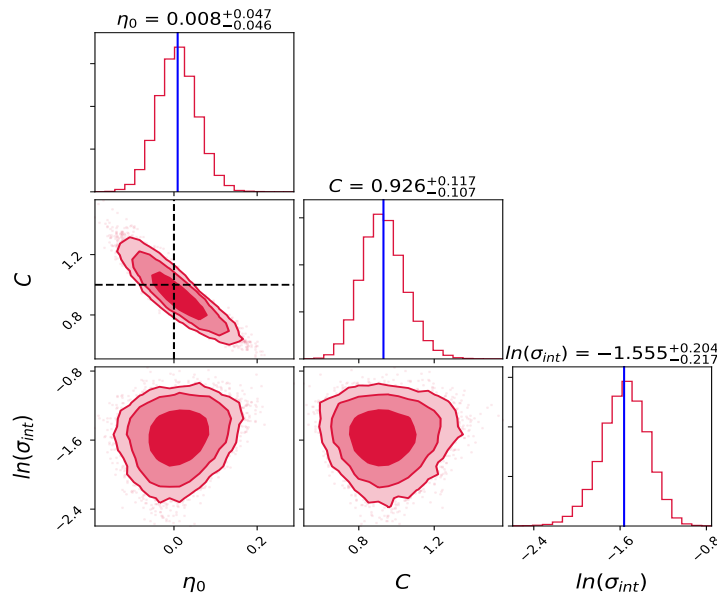


FIG. 5: **Case I:** Constraints on the parameters η_0 and C along with $\ln(\sigma_{int})$. The plots along the diagonal are the one-dimensional marginalized likelihood distributions. The contour plot represents the two-dimensional marginalized constraints showing the 68%, 95%, and 99% credible regions. These contours have been obtained using the `Corner` python module [96].

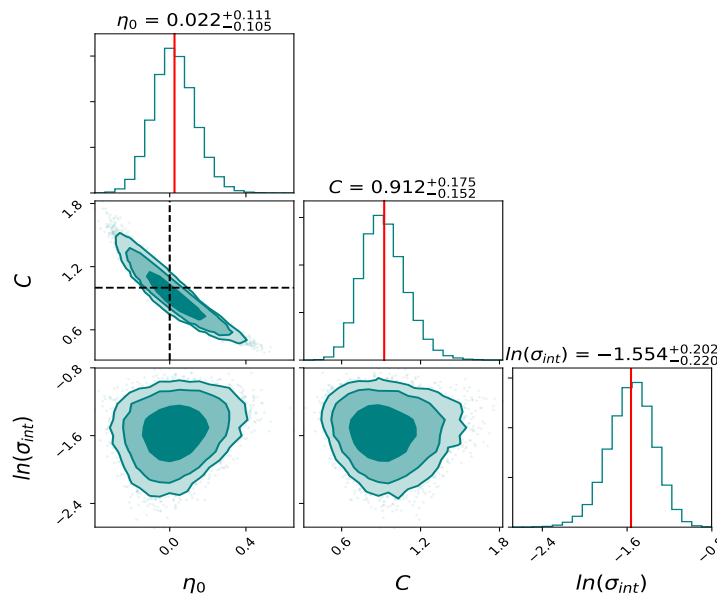


FIG. 6: **Case II:** Constraints on the parameters η_0 and C along with $\ln(\sigma_{int})$. The plots along the diagonal are the one-dimensional marginalized likelihood distributions. The contour plot represents the two-dimensional marginalized constraints showing the 68%, 95%, and 99% credible regions. These contours have been obtained using the `Corner` python module [96].

- [22] X.-L. Meng, T.-J. Zhang, H. Zhan, and X. Wang, *Astrophys. J.* **745**, 98 (2012), 1104.2833.
- [23] G. F. R. Ellis, R. Poltis, J.-P. Uzan, and A. Weltman, *Phys. Rev. D* **87**, 103530 (2013), URL <https://link.aps.org/doi/10.1103/PhysRevD.87.103530>.
- [24] K. Liao, Z. Li, S. Cao, M. Biesiada, X. Zheng, and Z.-H. Zhu, *Astrophys. J.* **822**, 74 (2016), 1511.01318.
- [25] M.-Z. Lv and J.-Q. Xia, *Physics of the Dark Universe* **13**, 139 (2016), 1606.08102.
- [26] X. Li and H.-N. Lin, *Mon. Not. R. Astron. Soc.* **474**, 313 (2018), 1710.11361.
- [27] H.-N. Lin, M.-H. Li, and X. Li, *Mon. Not. R. Astron. Soc.* **480**, 3117 (2018), 1808.01784.
- [28] C.-Z. Ruan, F. Melia, and T.-J. Zhang, *Astrophys. J.* **866**, 31 (2018), 1808.09331.
- [29] M.-Z. Lyu, Z.-X. Li, and J.-Q. Xia, *Astrophys. J.* **888**,

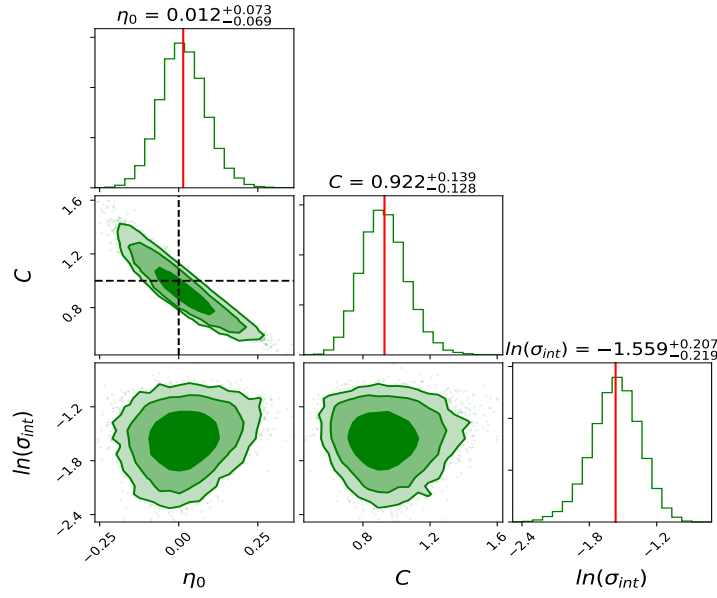


FIG. 7: **Case III:** Constraints on the parameters η_0 and C along with $\ln(\sigma_{int})$. The plots along the diagonal are the one-dimensional marginalized likelihood distributions. The contour plot represents the two-dimensional marginalized constraints showing the 68%, 95%, and 99% credible regions. These contours have been obtained using the `Corner` python module [96].

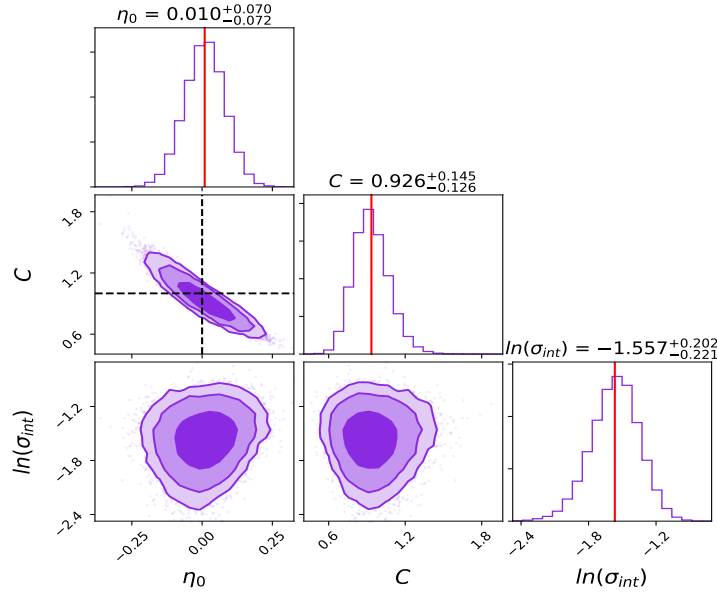


FIG. 8: **Case IV:** Constraints on the parameters η_0 and C along with $\ln(\sigma_{int})$. The plots along the diagonal are the one-dimensional marginalized likelihood distributions. The contour plot represents the two-dimensional marginalized constraints showing the 68%, 95%, and 99% credible regions. These contours have been obtained using the `Corner` python module [96].

- 32 (2020).
- [30] R. Arjona, JCAP **2020**, 009 (2020), 2002.12700.
- [31] S. W. Allen, A. E. Evrard, and A. B. Mantz, Ann. Rev. Astron. Astrophys. **49**, 409 (2011), 1103.4829.
- [32] A. V. Kravtsov and S. Borgani, Ann. Rev. Astron. Astrophys. **50**, 353 (2012), 1205.5556.
- [33] A. A. Vikhlinin, A. V. Kravtsov, M. L. Markevich, R. A. Sunyaev, and E. M. Churazov, Physics Uspekhi **57**, 317-341 (2014).
- [34] S. Desai, Physics Letters B **778**, 325 (2018), 1708.06502.
- [35] E. D. Reese, J. E. Carlstrom, M. Joy, J. J. Mohr, L. Grego, and W. L. Holzapfel, Astrophys. J. **581**, 53 (2002), astro-ph/0205350.
- [36] R. F. L. Holanda, J. A. S. Lima, and M. B. Ribeiro, Astrophys. J. Lett. **722**, L233 (2010), 1005.4458.
- [37] M. Hicken, W. M. Wood-Vasey, S. Blondin, P. Challis,

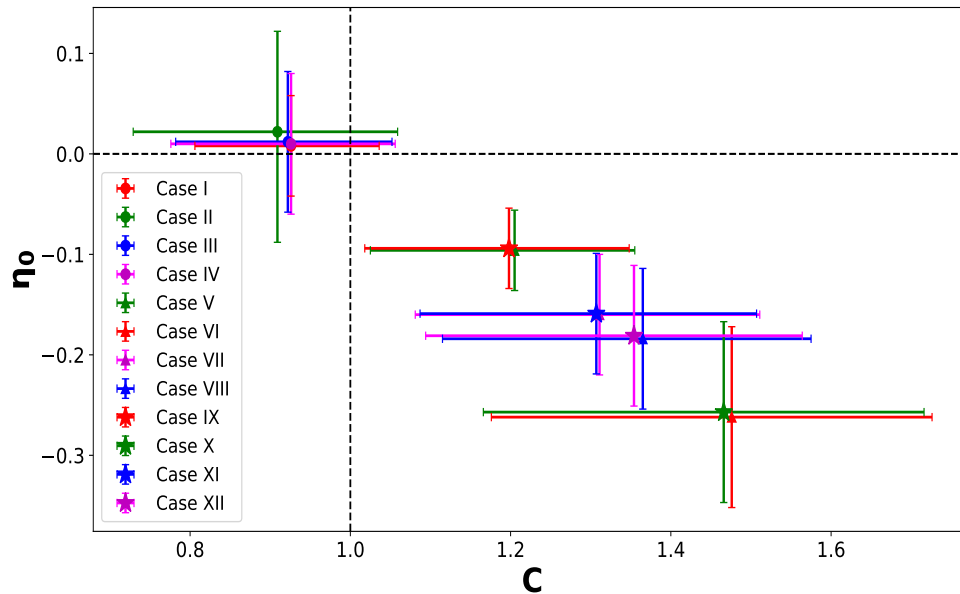


FIG. 9: A comparison of different cases studied in this work. The black dashed lines $(C, \eta_0) = (1, 0)$ correspond to the standard distance duality relation. A combination of different colors with different data style represent all different cases used in this study.

- S. Jha, P. L. Kelly, A. Rest, and R. P. Kirshner, *Astrophys. J.* **700**, 1097 (2009), 0901.4804.
- [38] S. J. LaRoque, M. Bonamente, J. E. Carlstrom, M. K. Joy, D. Nagai, E. D. Reese, and K. S. Dawson, *Astrophys. J.* **652**, 917 (2006), astro-ph/0604039.
- [39] S. Ettori, A. Morandi, P. Tozzi, I. Balestra, S. Borgani, P. Rosati, L. Lovisari, and F. Terenzi, *Astron. & Astrophys.* **501**, 61 (2009), 0904.2740.
- [40] R. S. Gonçalves, R. F. L. Holanda, and J. S. Alcaniz, *Mon. Not. R. Astron. Soc.* **420**, L43 (2012), 1109.2790.
- [41] R. Amanullah, C. Lidman, D. Rubin, G. Aldering, P. Astier, K. Barbary, M. S. Burns, A. Conley, K. S. Dawson, S. E. Deustua, et al., *Astrophys. J.* **716**, 712 (2010), 1004.1711.
- [42] R. F. L. Holanda, R. S. Gonçalves, and J. S. Alcaniz, *JCAP* **2012**, 022 (2012), 1201.2378.
- [43] N. Liang, Z. Li, P. Wu, S. Cao, K. Liao, and Z.-H. Zhu, *Mon. Not. R. Astron. Soc.* **436**, 1017 (2013), 1104.2497.
- [44] M. Bonamente, M. K. Joy, S. J. LaRoque, J. E. Carlstrom, E. D. Reese, and K. S. Dawson, *Astrophys. J.* **647**, 25 (2006), astro-ph/0512349.
- [45] X. Yang, H.-R. Yu, Z.-S. Zhang, and T.-J. Zhang, *Astrophys. J. Lett.* **777**, L24 (2013), 1310.0869.
- [46] E. De Filippis, M. Sereno, M. W. Bautz, and G. Longo, *Astrophys. J.* **625**, 108 (2005), astro-ph/0502153.
- [47] S. Santos-da-Costa, V. C. Busti, and R. F. L. Holanda, *JCAP* **2015**, 061 (2015), 1506.00145.
- [48] R. F. L. Holanda and S. H. Pereira, *Phys. Rev. D* **94**, 104037 (2016), 1610.01512.
- [49] N. Suzuki, D. Rubin, C. Lidman, G. Aldering, R. Amanullah, K. Barbary, L. F. Barrientos, J. Botyanszki, M. Brodwin, N. Connolly, et al., *Astrophys. J.* **746**, 85 (2012), 1105.3470.
- [50] G. Luzzi, M. Shimon, L. Lamagna, Y. Rephaeli, M. De Petris, A. Conte, S. De Gregori, and E. S. Battistelli, *Astrophys. J.* **705**, 1122 (2009), 0909.2815.
- [51] G. Hurier, N. Aghanim, M. Douspis, and E. Pointecouteau, *Astron. & Astrophys.* **561**, A143 (2014), 1311.4694.
- [52] R. F. L. Holanda, V. C. Busti, F. S. Lima, and J. S. Alcaniz, *JCAP* **2017**, 039 (2017), 1611.09426.
- [53] R. F. L. Holanda, S. H. Pereira, V. C. Busti, and C. H. G. Bessa, *Classical and Quantum Gravity* **34**, 195003 (2017), 1705.05439.
- [54] R. F. L. Holanda, L. R. Colaço, S. H. Pereira, and R. Silva, *JCAP* **2019**, 008 (2019), 1904.01342.
- [55] Planck Collaboration, P. A. R. Ade, N. Aghanim, M. Arnaud, M. Ashdown, J. Aumont, C. Baccigalupi, A. Balbi, A. J. Bandy, R. B. Barreiro, et al., *Astron. & Astrophys.* **536**, A11 (2011), 1101.2026.
- [56] D. M. Scolnic, D. O. Jones, A. Rest, Y. C. Pan, R. Chornock, R. J. Foley, M. E. Huber, R. Kessler, G. Narayan, A. G. Riess, et al., *Astrophys. J.* **859**, 101 (2018), 1710.00845.
- [57] W. J. C. da Silva, R. F. L. Holanda, and R. Silva, *Phys. Rev. D* **102**, 063513 (2020), 2005.04131.
- [58] A. B. Mantz, S. W. Allen, R. G. Morris, D. A. Rapetti, D. E. Applegate, P. L. Kelly, A. von der Linden, and R. W. Schmidt, *Mon. Not. R. Astron. Soc.* **440**, 2077 (2014), 1402.6212.
- [59] R. A. Sunyaev and Y. B. Zeldovich, *Comments on Astrophysics and Space Physics* **4**, 173 (1972).
- [60] M. Birkinshaw, *Physics Reports* **310**, 97 (1999), astro-ph/9808050.
- [61] J. E. Carlstrom, G. P. Holder, and E. D. Reese, *Ann. Rev. Astron. Astrophys.* **40**, 643 (2002), astro-ph/0208192.

- [62] T. Mroczkowski, D. Nagai, K. Basu, J. Chluba, J. Sayers, R. Adam, E. Churazov, A. Crites, L. Di Mascolo, D. Eckert, et al., *Space Science Reviews* **215**, 17 (2019), 1811.02310.
- [63] K. Bora and S. Desai, *Journal of Cosmology and Astroparticle Physics* **2021**, 012 (2021), 2008.10541, URL <https://doi.org/10.1088/1475-7516/2021/02/012>.
- [64] C. L. Sarazin, *Reviews of Modern Physics* **58**, 1 (1986).
- [65] A. V. Kravtsov, A. Vikhlinin, and D. Nagai, *Astrophys. J.* **650**, 128 (2006), astro-ph/0603205.
- [66] S. Galli, *Phys. Rev. D* **87**, 123516 (2013), 1212.1075.
- [67] L. R. Colaço, R. F. L. Holanda, R. Silva, and J. S. Alcaniz, *JCAP* **2019**, 014 (2019), 1901.10947.
- [68] A. Hees, O. Minazzoli, and J. Larena, *Phys. Rev. D* **90**, 124064 (2014), 1406.6187.
- [69] R. S. Gonçalves, S. Landau, J. S. Alcaniz, and R. F. L. Holanda, *JCAP* **2020**, 036 (2020), 1907.02118.
- [70] O. Minazzoli and A. Hees, *Phys. Rev. D* **90**, 023017 (2014), 1404.4266.
- [71] E. Rozo, A. Vikhlinin, and S. More, *Astrophys. J.* **760**, 67 (2012), 1202.2150.
- [72] S. Planelles, D. Fabjan, S. Borgani, G. Murante, E. Rasia, V. Biffi, N. Truong, C. Ragone-Figueroa, G. L. Granato, K. Dolag, et al., *Mon. Not. R. Astron. Soc.* **467**, 3827 (2017), 1612.07260.
- [73] V. Biffi, F. Sembolini, M. De Petris, R. Valdarnini, G. Yepes, and S. Gottlöber, *Mon. Not. R. Astron. Soc.* **439**, 588 (2014), 1401.2992.
- [74] D. Fabjan, S. Borgani, E. Rasia, A. Bonafede, K. Dolag, G. Murante, and L. Tornatore, *Mon. Not. R. Astron. Soc.* **416**, 801 (2011), 1102.2903.
- [75] S. T. Kay, M. W. Peel, C. J. Short, P. A. Thomas, O. E. Young, R. A. Battye, A. R. Liddle, and F. R. Pearce, *Mon. Not. R. Astron. Soc.* **422**, 1999 (2012), 1112.3769.
- [76] R. Stanek, E. Rasia, A. E. Evrard, F. Pearce, and L. Gazzola, *Astrophys. J.* **715**, 1508 (2010), 0910.1599.
- [77] C. Loken, M. L. Norman, E. Nelson, J. Burns, G. L. Bryan, and P. Motl, *Astrophys. J.* **579**, 571 (2002), astro-ph/0207095.
- [78] E. Bulbul, I. N. Chiu, J. J. Mohr, M. McDonald, B. Benson, M. W. Bautz, M. Bayliss, L. Bleem, M. Brodwin, S. Bocquet, et al., *Astrophys. J.* **871**, 50 (2019), 1807.02556.
- [79] J. E. Carlstrom, P. A. R. Ade, K. A. Aird, B. A. Benson, L. E. Bleem, S. Busetti, C. L. Chang, E. Chauvin, H. M. Cho, T. M. Crawford, et al., *PASP* **123**, 568 (2011), 0907.4445.
- [80] L. E. Bleem, B. Stalder, T. de Haan, K. A. Aird, S. W. Allen, D. E. Applegate, M. L. N. Ashby, M. Bautz, M. Bayliss, B. A. Benson, et al., *Astrophys. J. Suppl. Ser.* **216**, 27 (2015), 1409.0850.
- [81] S. Bocquet, J. P. Dietrich, T. Schrabback, L. E. Bleem, M. Klein, S. W. Allen, D. E. Applegate, M. L. N. Ashby, M. Bautz, M. Bayliss, et al., *Astrophys. J.* **878**, 55 (2019), 1812.01679.
- [82] A. Saro, S. Bocquet, E. Rozo, B. A. Benson, J. Mohr, E. S. Rykoff, M. Soares-Santos, L. Bleem, S. Dodelson, P. Melchior, et al., *Mon. Not. R. Astron. Soc.* **454**, 2305 (2015), 1506.07814.
- [83] S. Desai, R. Armstrong, J. J. Mohr, D. R. Semler, J. Liu, E. Bertin, S. S. Allam, W. A. Barkhouse, G. Bazin, E. J. Buckley-Geer, et al., *Astrophys. J.* **757**, 83 (2012), 1204.1210.
- [84] J. Song, A. Zenteno, B. Stalder, S. Desai, L. E. Bleem, K. A. Aird, R. Armstrong, M. L. N. Ashby, M. Bayliss, G. Bazin, et al., *Astrophys. J.* **761**, 22 (2012), 1207.4369.
- [85] M. Arnaud, G. W. Pratt, R. Piffaretti, H. Böhringer, J. H. Croston, and E. Pointecouteau, *Astron. & Astrophys.* **517**, A92 (2010), 0910.1234.
- [86] J. B. Melin, J. G. Bartlett, J. Delabrouille, M. Arnaud, R. Piffaretti, and G. W. Pratt, *Astron. & Astrophys.* **525**, A139 (2011), 1001.0871.
- [87] N. Battaglia, J. R. Bond, C. Pfrommer, J. L. Sievers, and D. Sijacki, *Astrophys. J.* **725**, 91 (2010), 1003.4256.
- [88] M. Seikel, C. Clarkson, and M. Smith, *JCAP* **2012**, 036 (2012), 1204.2832.
- [89] H. Singirikonda and S. Desai, *European Physical Journal C* **80**, 694 (2020), 2003.00494.
- [90] K. Bora and S. Desai, arXiv e-prints arXiv:2103.12695 (2021), 2103.12695.
- [91] F. Pedregosa, G. Varoquaux, A. Gramfort, V. Michel, B. Thirion, O. Grisel, M. Blondel, P. Prettenhofer, R. Weiss, V. Dubourg, et al., *Journal of Machine Learning Research* **12**, 2825 (2011).
- [92] E.-K. Li, M. Du, Z.-H. Zhou, H. Zhang, and L. Xu, *Mon. Not. R. Astron. Soc.* **501**, 4452 (2021), 1911.12076.
- [93] R. Jimenez and A. Loeb, *Astrophys. J.* **573**, 37 (2002), astro-ph/0106145.
- [94] D. Foreman-Mackey, D. W. Hogg, D. Lang, and J. Goodman, *PASP* **125**, 306 (2013), 1202.3665.
- [95] X.-Y. Fu, P.-X. Wu, H.-W. Yu, and Z.-X. Li, *Research in Astronomy and Astrophysics* **11**, 895 (2011).
- [96] D. Foreman-Mackey, *The Journal of Open Source Software* **1**, 24 (2016), URL <https://doi.org/10.21105/joss.00024>.